Supplementary Material

Climate change through the essentials – nature's offering and humankind's sine qua non

Thomas Anderl*

*** Correspondence:** Thomas Anderl: bhu.research@gmx.net

S1. Proportionality of longwave absorption to number densities

The influence of atmospheric CO_2 on the (global annual mean) surface temperature has been derived from measurements through Earth's history, particularly the period of 35-50 million years ago [1]. The result is a simple function of (equilibrated) temperature in dependence on the atmospheric CO_2 concentration. This function, termed the 'Eocene relationship', includes all entailed effects, e.g., from water vapor.

This function, in turn, has been used to examine the relationship to the underlying particle (number) densities (throughout the present descriptions, particle (number) density and mixing ratio synonymized with concentration). In the previous analysis, the atmospheric absorption of surface radiation, amounting to 57 W/m^2, has been related to the compound concentrations of atmospheric CO_2 and H_2O [2]. It has been found that the absorption appears proportional to the concentrations of the two species.

Relating the compound concentrations of the two species to the absorption of 57 W/m^2 is probably an oversimplification, as CO_2 and H_2O exhibit different absorption characteristics. Therefore, the absorption-concentration relationship is examined separately for the two species on the following basis. The variation of the CO_2 concentration with temperature is taken from the Eocene relationship. The H_2O concentration is taken to exponentially vary with temperature according to the Clausius Clapeyron relationship, i.e., by 7 %/°C, starting with 0.4 % at preindustrial conditions. The absorbed radiation is first viewed proportional to the concentrations, at preindustrial conditions amounting to 18 and 5 W/m^2 for CO_2 and H_2O, respectively; then, the absorption of CO_2 is reduced by 1.8 % per 100 ppmv to take saturation into account. Furthermore, the absorbed radiation is taken as proportional to the Planck blackbody radiation per wavelength unit for the wave numbers of 670 and 1,450 cm^{-1} representing CO_2 and H_2O, respectively; further wave number regimes are assumed of second order and hence disregarded.

In result, the proportionality-based temperature determination corresponds to the Eocene relationship within deviations of ±5.3 % for the surface temperature range of 13-31 °C and CO_2 concentration range of 242-3,600 ppmv. From 13 °C down to 11 °C, the deviation increases to 14 %, CO_2 ranging down to 180 ppmv. Thus, again, the absorbed radiation appears proportional to the concentrations of CO_2 and H_2O. The 18 and 5 W/m^2 of absorption at preindustrial conditions are interpreted to represent the concentration-dependent absorption determining the surface temperature variability. As result for instance, a 10 % rise of the CO_2 concentration causes the absorption to increase by 10 % of 18 W/m^2.

Out of curiosity, when looking for further simplification, it proves even possible to linearize the Eocene relationship: A change of the CO_2 concentration by 100 ppmv corresponds to an equilibrium surface temperature change of 2.1 °C within deviations of ±4.3 % from the

Eocene relationship for the temperature and CO_2 regime of 11-18 °C and 179-511 ppmv.

S2. Atmospheric CO_2 concentration

For projection of the atmospheric CO_2 concentration, the simplified approach described in [6] has been slightly adapted to a temperature dependency of soil heterotrophic respiration in the order of 3-4 GtC/year/°C [10-12] as well as to a CO_2 fertilization effect in terrestrial vegetation of about 2.5 GtC/year on average for the period 1990-2007 and natural tropical forest regrowth after deforestation [13], the latter approximated by 7 % of anthropogenic emissions.

The terrestrial vegetation dominates the projection of the atmospheric CO_2 concentration in Fig. 1 of the main article. In the present approach, the prevailing feature is the separate treatment of vegetational growth (net primary productivity, NPP) and carbon release from the ground in their dependencies on the surface temperature and the atmospheric CO_2 concentration. For instance, NPP increases with rising CO_2 concentration, known as the fertilization effect. The net uptake, i.e., the flux difference between NPP change and soil respiration change, is depicted in Fig. S1 in dependence on the atmospheric CO_2 concentration (horizontal axis) and the surface temperature (various lines) relative to the preindustrial conditions.

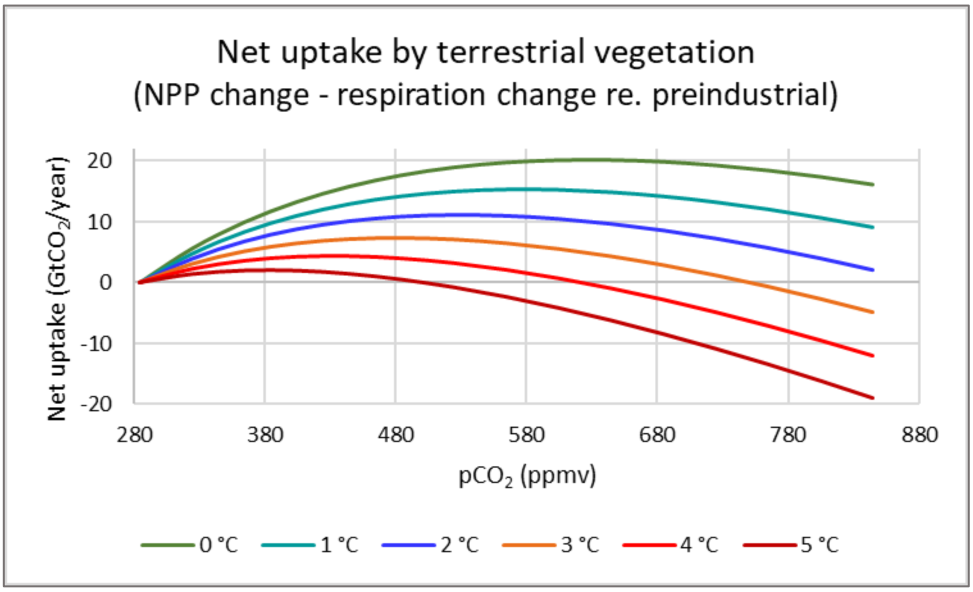

Fig. S1. Computation of the present work on the difference between NPP change and soil respiration change relative to preindustrial conditions in dependence on the atmospheric CO_2 concentration (pCO_2, horizontal axis) and (mean global annual) surface temperature change (various lines, 0 °C (upper line) to 5 °C (lowest line), legend self-explaining).

On the one hand, increase of soil carbon respiration with rising CO_2 concentration and temperature is sourced from the soil carbon stock. On the other hand, the net uptake is viewed to enter the soil carbon stock. From the present formalism, the latter appears to be well approximated by 50 % of NPP change, which is the base of the computation for Fig. 1 (main article). To understand the importance of this parameter, a computation has been performed with 25 % of NPP change filling the soil carbon stock, which approximately corresponds to the belowground biomass at the global average root:shoot ratio of 0.3 [7]. This would lead to a peak warming of 1.4 °C after preindustrial times for 2 %/year emissions reduction (cf. Fig. 1) and a sea level peak of roughly 3-4 m in year 2700 (cf. next chapter, sea level projection).

The entire CO_2 projection as depicted in Fig. 1 of the main article appears supported through the zero emissions case (black lines in Fig. 1) as the general trend corresponds well to the multi-study results of sophisticated models [14].

S3. Global sea level

S3.1 Sea level versus surface temperature – history

The left-hand side of Fig. S2 shows the observed sea levels (solid blue line) [1, 34] and temperatures (dashed orange line) [35-38] since the last glacial maximum. Sea level change velocities are indicated by dotted lines for 1.27 m/century during the major glacial-to-interglacial increase and for 0.2 m/century during the past 9,000 years. It appears like watching the sea level to typically lag temperature.

The right-hand side of Fig. S2 shows the results from observation-constrained simulations for the sea level dependency on the surface temperature relative to the present [39]. The solid lines represent the results of a 3-D model (red line, lower to the left) and a 1-D model (upper line, entire temperature range), centred around the present conditions. For ease of illustration, the published error bars are omitted from Fig. S2; they have been shown in the order of ±4 m for the temperature regime 0 to 5 °C and largest of ±20 m and ±10 m in the regime -8 to -12 °C and at 16 °C, respectively, for the given temperature scale [39].

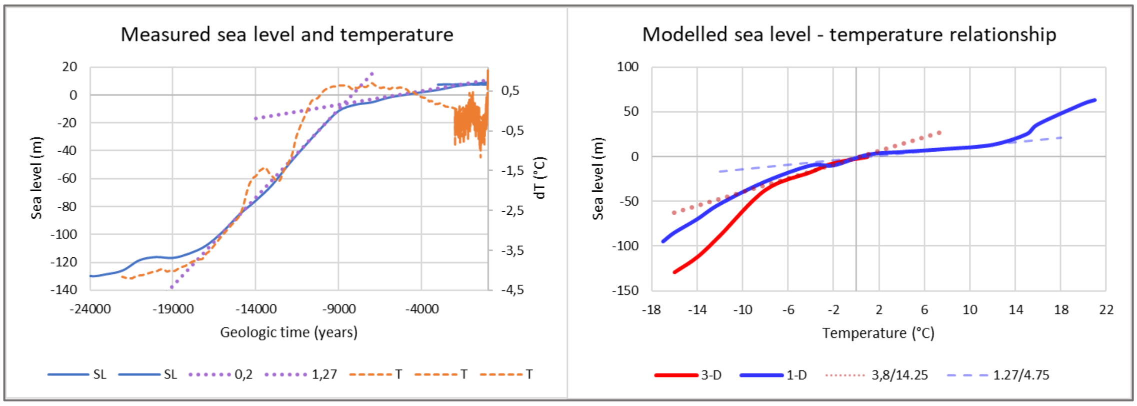

Fig. S2. Left: Measured sea level (solid blue line, left vertical scale) [1, 34] and temperature change (dashed orange line, right vertical scale) [35-38] through the past about 20,000 years; dotted straight lines for sea level slopes of 0.2 and 1.27 m/century (upper right and central, respectively). Right: Previously modelled sea level in dependence on reconstructed Northern surface temperature, translation to mean global surface temperature see text; 3-D model solid red line (lower left), 1-D model solid blue line (upper, entire temperature range), coarse reproduction of [39]; dotted straight line for slope 3.8 (14.25) m/°C, dashed straight line for slope 1.27 (4.75) m/°C for Northern (global) temperatures.

It can be inferred that the temperature scale shown (Fig. S2, right, horizontal axis) relates to the global annual mean surface temperature by division through 3.75 for the following reasons. First, the reconstructed Northern Hemisphere temperatures of the referenced publication (Fig. S2, right) exhibit a span of 15 °C over the past 450,000 years (Fig. 2 of [39]), whereas the span for the global mean surface temperature is generally comprehended as 4 °C, leading to the factor of 3.75. Second, the reconstructed temperatures amount to the order of 25 °C above the present temperature at approximately 25 million years ago (Fig. 4c of [39]), while consolidated data reveal a temperature of 6 °C [40].

The dotted and dashed lines (Fig. S2, right) depict a sea level-temperature dependency of 3.8 (14.25) and 1.27 (4.75) m/°C, respectively, the values before the brackets for the temperature scale in the figure and within the brackets for the corresponding mean global surface temperatures.

S3.2 Sea level versus ocean heat content and surface temperature – history

The blue line on the left-hand side in Fig. S3 shows the observed full-depth ocean heat content over the past 2,000 years (coarse reproduction of [41]) in comparison with the surface temperature [36-38]. The period until 600 CE (Common Era) is interpreted to exhibit

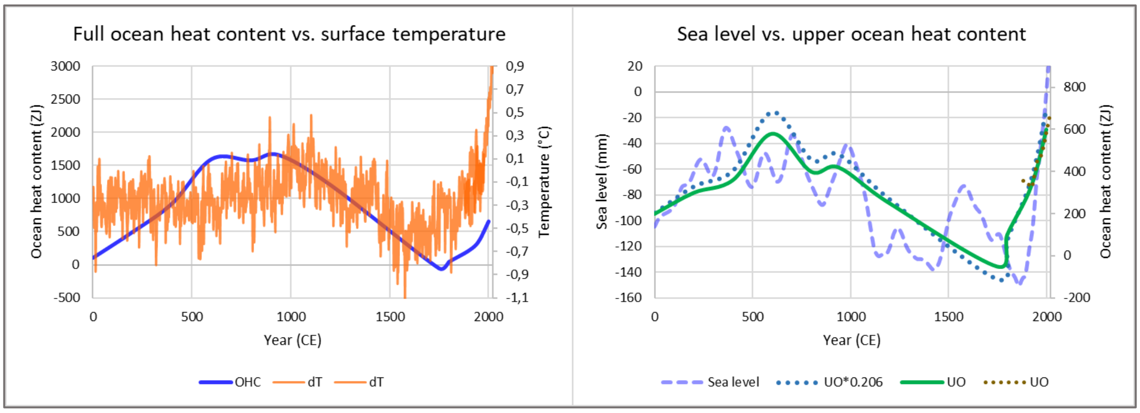

Fig. S3. Data for the past 2000 years. Left: Full-depth ocean heat content (OHC, smooth blue line, left vertical axis, coarse reproduction of [41]) and variability of the mean global annual surface temperature (wiggly orange line, right vertical axis) [36-38]. Right: Sea level (dashed blue line, left vertical axis) [34]; ocean heat content (right vertical axis): 0-700 m depth (UO) (solid green line [41], dotted purple line (barely visible to the right) [42]), UO times 0.206 (dotted blue line) for comparison with sea level.

continuous energy uptake by the oceans from strong insolation [6], leaving the surface temperature unchanged. Once ocean heat uptake stops at 600 CE, surface temperature increases, interpreted to reach equilibrium with ocean heat content at 1100 CE. Then, the surface and ocean temperatures decline synchronously – probably continuously through equilibrium states. Starting from the period 1600-1750, a strong surface temperature increase leaves the ocean heat content far behind. This requires deeper insight.

When comparing the full-depth ocean heat content (Fig. S3, left, blue line) with the observed sea level (Fig. S3, right, dashed blue line) [34] in the period 600-1750 CE, a difference of 1600 ZJ in ocean heat content approximately corresponds to 80 mm of sea level change, or 0.05 mm/ZJ. This is far below the common comprehension of 0.12-0.15 mm/ZJ [43]. As a resolution, it is interpreted that sea level change is dominated by heat content change in the upper ocean layer. For verification, the corresponding heat trend for 0-700 m depth is depicted by the solid green and dotted purple lines (UO) on the right-hand side of Fig. S3 [34, 41]. Multiplication of the upper ocean heat content (solid green line) by 0.2 yields the dotted blue line, reproducing the observed sea level trend (dashed blue line, Fig. S3, right). The factor of 0.2 is interpreted to be composed of 0.14 mm/ZJ for the thermosteric contribution (agreeing with 0.135 mm/ZJ for the upper 700 m in [44]) and 40 % of this for water mass increase from land snow/ice melting. Overall, the extracted values appear well in line with the general knowledge from sophisticated research. According to the present understanding, the halosteric effect plays a minor role (see below); in other words, the thermosteric component dominates the total steric effect.

A deeper look is now devoted to more basic terms by identifying effective ocean properties. From 600 to 1100-1750 CE, Fig. S3 reveals by an order of magnitude that an 80 mm sea level rise corresponds to changes of 630 ZJ in the upper ocean (UO) and 0.63 °C in surface temperature. This value set can be reproduced by the following averages: upper ocean layer depth 700 m, heat capacity 3,850 J/kg/°C, density 1,039 kg/m^3, expansion coefficient $130 \cdot 10^{-6}$ °C^{-1}, addition of 40 % for mass from snow/ice melting. This parametrization appears to be in good agreement with general knowledge and is consistent within itself.

The preceding descriptions characterize nature in preindustrial times. Until about 1975, the corresponding relationships were retained: 80 mm sea level rise, 630 ZJ relevant ocean heat gain, and 0.63 °C warming. This pattern changes after 1975: 63 mm sea level rise have happened with added 140 ZJ and 0.8 °C; thus, similar sea level rise and temperature gain as before (±25 %), however a factor of 4.5 lower ocean heat gain (in the dominating upper layer). This is regarded as an indication that, recently, temperature has driven sea level without much contribution from ocean warming, presumably dominated by snow/ice melting.

Zooming into the data since 1970, the ocean heat content has grown by about 4 ZJ/year. This is assumed to reflect the maximum pace owing to the energy exchange inertia of the upper ocean layer. With the figures related to the time before 1975, for instance, 1.4 °C warming corresponds to a gain of 1400 ZJ and would be reached during 350 years with a sea level contribution of approximately 0.18 m. The comparison with the expected total sea level velocity of about 0.5 m/century (see below) reveals that the future sea level rise will mainly be determined by snow/ice mass contribution, reducing the thermosteric (and steric) effect to about 10 %.

S3.3 Sea level projection – future

According to the right-hand side of Fig. S2, sea level will follow the gentle increase with temperature (4.75 m/°C) until 2.5-3 °C global average warming from the present. At higher temperatures, the dependency jumps to a tremendous 25.5 m/°C. These values form the basis of the present analysis (results as blue lines in Fig. S4).

According to the left-hand side of Fig. S2, the sea level pace was 0.2 m/century for many thousand years until the present. For the past 30 years, however, sea level has risen virtually along a straight line at approximately 0.34 m/century [45]. According to the present understanding, inertia, particularly from ice melting, sets an upper limit on sea level rise velocity. The previous 0.2 m/century will probably be too low for the future since the past rise has happened at decreasing temperatures, interpreted that nature has been transitioning to a new, not yet achieved, equilibrium (Fig. S2, left). As mentioned, 0.34 m/century is the present pace. It turns out that using the above 4.75 m/°C, limiting velocity in the range 0.2-0.6 m/century, and applying this to the 2 %/year emissions reduction scenario of the main article (solid green lines in Fig. 1), the results are in accordance with previous publications [46-50], depicted for one instance by the short-dashed red line in Fig. S4.

In Fig. S4, the temperature projection from the main article is repeated as a solid green line (left vertical axis) together with the corresponding results for sea level rise (right vertical axis). The expert elicitation reported in [50] exhibits a sea level velocity increase with surface temperature by 0.42 m/century/°C (error +0.31, -0.09). This applied to the green temperature trend yields the sea levels depicted by the short-dashed red line in Fig. S4. This is compared with the present simplified approach of 4.75 m/°C with a limit in the range of 0.3-0.5 m/century (blue lines in Fig. S4, labelled accordingly: dotted, long-dashed, solid for 0.3, 0.4, and 0.5 m/century, respectively). In conclusion, a 5-6 m sea level rise needs to be accounted for until 3100 CE, returning afterwards.

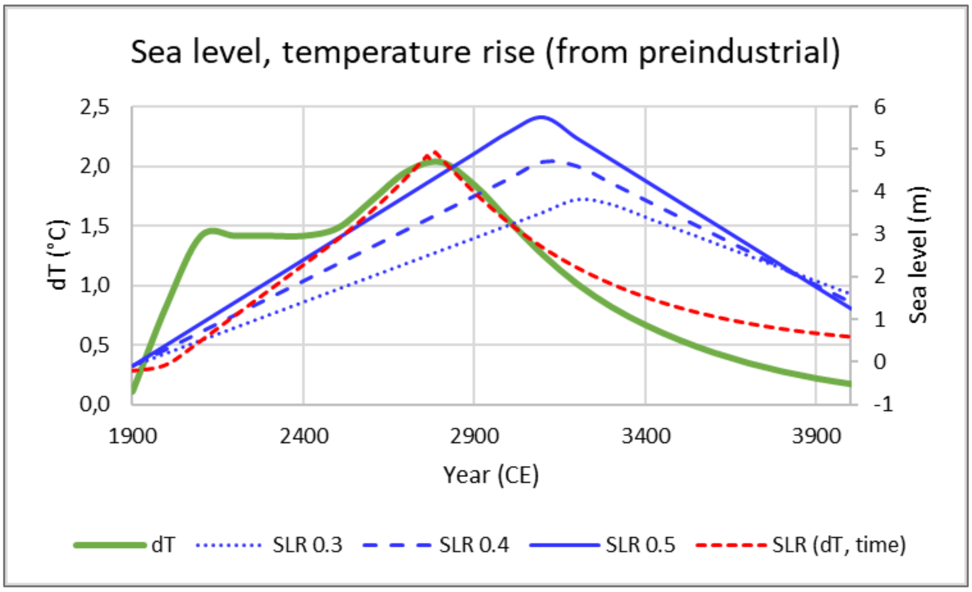

Fig. S4. Temperature change (dT, left vertical axis) and sea level change (right vertical axis) for the past 120 years with projection for ca. 2000 years, present computation. Temperature as derived in the main article for a CO_2 emissions reduction of 2 %/year relative to the present (solid green, copy from Fig. 1 in the main article). Corresponding sea level estimation in dependence on temperature (see text) and with maximum change velocity of 0.3 (SLR 0.3, dotted blue), 0.4 (SLR 0.4, long-dashed blue), 0.5 (SLR 0.5, solid blue) m/century, and velocity-temperature-time dependency according to [50] (short-dashed red).

S4. Regional sea level

Global sea level variability (preceding discussion) is superimposed with local vertical land motion. Specifically, global sea level is determined by density (steric) effects and mass effects (particularly from land snow/ice melting and land ground water release); local contributions are dominated by changes in ice weight (glacial isostatic adjustment), densification of land mass (natural and from buildings), and resource exploitation (particularly of fossils and ground water). Steric contributions are generally subdivided into the effects of temperature (thermosteric) and salt concentration (halosteric). For a basic understanding, the halosteric contribution may be considered to primarily originate in temperature; for instance, fresh water is added to the oceans from polar ice melting in the tail of a temperature increase. Furthermore, the halosteric contribution is viewed as subordinate to the thermosteric contribution [51]. In addition, the global sea level rise from land ground-water extraction is considered negligible. In the preceding chapter [S3], global sea level variability was examined in terms of its compound dependency on surface temperature and ocean heat content. Subsequently, the contributions from vertical land motion are considered.

Previous research has partly focused on total land motion and partly separated the contribution from glacial isostatic adjustment. Selected results for the current compound downward land (subsidence) velocities are 1.6 m/century for the Mekong Delta [52], 1-3 m/century for Bangkok [53], 3-10 m/century for Jakarta [54], and locally up to 19-28 m/century in Jakarta, Bandung, and Semarang (Indonesia) [55].

Approximately ¼ of the 51 largest coastal cities previously studied have a median subsidence rate exceeding 0.2 m/century [56]. Chittagong (Bangladesh) is revealed as the place with the highest impact on population. For the present, the median of land downward motion is given as 1.2 m/century. The population is forecasted to grow by a factor of 3.3 from the present to 2100 [57]. In the projection for 2050, vertical land motion is found to amplify the land affected by global sea level rise by a factor of 2.2 and the affected population by 2.4 [56]. Here, extrapolating the impact into the future, taking 0.5 m/century as global sea rise (cf. Fig. S4) and half of the population growth affected, the local land motion will amplify the population-related impact from global sea level rise by a factor of 2.7 at year 2100.

In a study covering large towns on the east coast of China, glacial isostatic adjustment was separated from vertical land motion [58]. As result, the residual land motion contributes up to 90 % of global sea level rise (i.e., in addition to global sea level rise).

S5. Disastrous events

Heat waves. Principally, warmer temperatures are expected to be accompanied by an increase in the frequency and strength of heat waves. Actual significant strengthening of the heat waves should be reflected by a clear signal in the measurement data. For an analysis, the frequently used data sets HadEX3 and GHCNDEX are examined at the global level [59, 60] – the former reaching back to 1900 with strong concentration in North European regions, the latter starting in 1951 with additional regional focus, for instance, in North America.

Fig. S5a shows the measured temperatures from 1900 as a light-green line [61]. The general pattern reveals two rising phases: the first (smaller) from about 1910 to 1940, the second (stronger) from 1975 onwards. The solid blue and dashed red lines represent measurements of the number of days per year with at least six consecutive days exhibiting temperatures within the highest 10 % of the period 1961-1990. First, the patterns with a North European focus (solid blue) and additional regions (dashed red) are revealed to be similar. Second, before 1940, the heat wave indicator followed the temperature. In contrast, during 1940-1975, the heat wave indicator shrunk to 1910-levels while the temperature remained quite high. After 1975, heat wave strength and temperature have risen in common, and the heat wave indicator seemingly catches up with temperature, both clearly exceeding the 1930s highs. Third, from the first impression, a significant change in the heat wave frequency is unsupported. The length of the heat waves has exhibited a larger spread after 1995 than before.

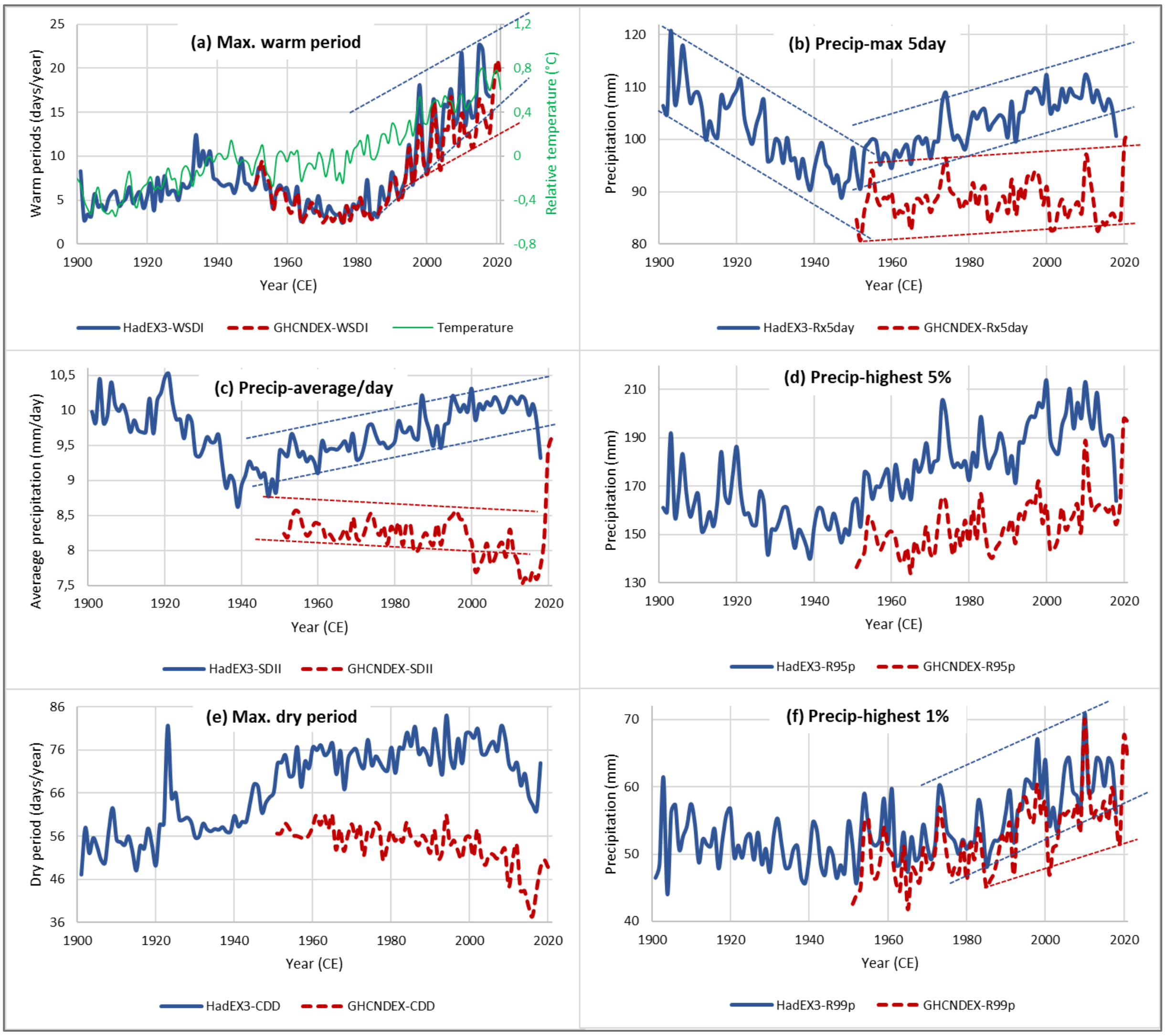

Fig. S5. Extreme-weather indicators from temperature and precipitation measurements [59-61], related reference period 1961-1990 (RP); solid blue: HadEX3 data set, dashed red: GHCNDEX data set; dotted straight lines to guide the eye. (a) number of days per year with at least six consecutive days of temperatures in the highest 10 % of RP, with temperature measurements (light solid green line); (b) maximum consecutive 5-day precipitation per year; (c) average daily precipitation per year; (d) annual precipitation when daily precipitation in the highest 5 % of RP; (e) maximum number of consecutive dry days per year; (f) annual precipitation when daily precipitation in the highest 1 % of RP.

Extreme rainfall. Precipitation is anticipated to follow temperature to a certain extent. As a general indicator, the average precipitation per day showed opposing trends for the two data sets (Fig. S5c) and moreover, the average daily precipitation has remained within the variability of the last century for the long-term data, probably indicating the natural variability. Recently, a big jump may have appeared, which is subject to statistical confirmation in the future. A trend in cyclic frequency change appears hard to be inferred.

In addition, droughts are generally expected to follow rising temperatures. The maximum number of consecutive dry days per year is shown in Fig. S5e. Again, the two data sets exhibit opposite trends; the long-term measurements remain within the century variability, and cyclic frequency changes are inapparent.

Furthermore, higher temperatures increase the probability of heavy rain events [4]. The right half of Fig. S5 shows three indicators of the two data sets: the maximum 5-day precipitation per year (Fig. S5b); the annual precipitation when daily precipitation lies in the highest 5 % (Fig. S5d) and 1 % (Fig. S5f) of the period 1961-1990. In short, a clear signal can be detected in the latter indicator (Fig. S5f). The indicator starts increasing at approximately 1975 in line with temperature (Fig. S5a, light green), both precipitation data sets reveal a coherent upward trend after 1975 (by about 3 %/decade) with a tendency to leave the (predominantly natural) variability range of the 20th century in the present century. A change in cycle frequency is unapparent. A viable question is which values in the maxima of the highest precipitation events must be considered disastrous. In presumably almost preindustrial conditions until about 1965, the maxima were at 60 mm (Fig. S5f). Are magnitudes above 60 mm disastrous, or already somewhere below 60 mm disastrous? Compared with extreme floods during the past 150 years [15], a threshold may be inferred at 55 mm for the indicator in Fig. S5f. In this case, the frequency of extreme events has risen above the preceding levels since 1983. However, regarding extreme floods in Europe during the past 500 years, no clear particularities can be inferred for the past several decades [16]. A further idea is that the 10-years rolling average of the 1 %-highest precipitation (base data of Fig. S5f) is a good indicator of the combined strength of frequency and magnitude. From this, an upward trend of 6 %/decade (arithmetic) may be detected for strong precipitation events during the period 1987-2018 (cf. supplementary data and code). In summary, strong precipitation have recently increased by about 3-6 %/decade which translates into 16.7-33.3 %/°C with a temperature rise of 0.18 °C/decade during the same period of time.

It should be noted that the observations on the past do not preclude juvenile trends. The corresponding inferences and projections must rely on simulations first. Furthermore, the present spatially coarse consideration is perceived as a good indicator of overall probabilities, leaving room for regional specifics.

S6. Mitigation potentials and costs

S6.1 Mitigation potentials and costs

The results of [8] for the CO_2 emissions mitigation potentials and related costs are summarized in Table S1. Data from [62] relate to a projection for the period 2010-2030 and are presumed applicable until the present; a verification or update is subject to future studies. In total, 10.1 GtC/year are revealed abatable at neutral cost, i.e., investments and operational costs in the abated world equal those of the present non-abated world. The mitigation potential reflects 92 % of current total emissions.

S6.2 Electricity storage costs in the renewables' world

Within the derivation of cost-neutrality for approximately 90 % of CO_2 abatement, the present levelized cost framework for energy supply disregards the necessity of storage in the renewables' world [8]. A study on Germany has concluded that 100 % energy supply by renewables is possible at levelized costs unchanged relative to the present [63].

Detailed insight into the same study reveals future 100 % renewables energy generation by 4 c/kWh (Eurocent) more expensive in year 2025 than in the fossil-dominated period until 2018, the surcharge gradually vanishing until 2040 [64]. In a further study related to Germany, battery storage needs are expected to amount to approximately 3 c/kWh in photovoltaic installations, except for small rooftop systems with a storage demand of 6 c/kWh [65].

Sector	**Abatement potential ($GtCO_2$/year)**	**Abatement cost (GEuro/year)**	**Source**
Electricity generation	3.5	0	Abatement potential without CCS [62]; levelized cost determination and field experience [8]
Forestry - Reduced deforestation, reduced agriculture - Afforestation, reforestation	 1.3 1.1	 40.5 164.1	 [62] 350 Mha afforestation [8], abatement [7], 469 Euro/ha/year cost
Agriculture	1.2	-6.0	[62]
Buildings	0.9	-121.5	[62]
Transport	0.6	-22.3	[62]
Chemicals	0.4	-11.6	[62] without CCS
Waste	0.4	-16.7	[62]
Cement	0.3	-0.1	[62]
Iron, steel	0.2	-9.4	[62] without CCS
Petroleum, gas	0.2	-17.0	[62] without CCS
Total	**10.1**	**0**	**Abatement 92 % of global 11 GtC/year from fossil fuel, industry, and land use**

Table S1. CO_2 abatement potentials and related costs, according to [8] and partly reusing [62].

In the case of 4 c/kWh extra cost for storage (here for simplicity, c for US$-cent and Eurocent): In the USA, the required storage would raise current retail electricity prices from 12 to 15 c/kWh, with anticipated effects from the Inflation Reduction Act incorporated [66]. In Europe, current residential electricity prices are on average 25.2 c/kWh in the purchase power standard (electricity cost in relation to other goods and services) comprising 1.5 and 3.8 c/kWh for energy and VAT taxes, respectively [67]; thus, tax exemption can readily avoid a potential price increase due to the storage needs.

S6.3 Investment relocation from fossil fuels to renewables energy generation

Current investments in fossil fuel supply and fossil fuel power generation are in the order of $ 800 billion per year ($ for US$), at present (year 2016) as well as on average for the period 2000-2016 [68]. Levelized cost composed of capital, grid integration, and storage per generated kWh has been derived as 10.1, 13, and 17.3 c/kWh for onshore wind, PV (photovoltaic), and offshore wind, respectively (values of [8] plus the above 4 c/kWh for storage). For simplicity, photovoltaic is viewed as a good indicator for a realistic mix average. Fossil fuel end-use energy supply is taken as 110 TWh/year at present. If half of the fossil fuel-related investments (400 bn$/year) are redirected every year to renewables (PV as representative of PV-wind mixtures), 3 % of total fossil-based energy supply is incrementally replaced year by year. Taking 77 % of total CO_2 emissions to originate from fossil usage (the rest primarily from land use and cement manufacture [5] and 90 % of fossil emissions being omitted by renewables [8], the 3 %/year replacement results in a reduction of 2 %/year of total CO_2 emissions.

S7. CO_2 emissions and economic activity

This section examines the dominant relationships between CO_2 emissions and economic activity. The considered variables are population, GDP, energy consumption, CO_2 emissions, and associated derivatives per capita, per unit of GDP, and per unit of energy consumption. The solid blue lines in Fig. S6 show their temporal trends. While some curves are apparent as exponential (for example, GDP, Fig. S6c, and CO_2 emissions, Fig. S6d), others appear linear (for example, population, Fig. S6a, and energy consumption, Fig. S6b). To simplify the analysis, all temporal trends are taken as exponential with a constant annual change rate each, and the results are depicted by the dashed orange lines in Fig. S6.

The interrelationships supposedly adhere to a multi-equation system for the annual change rates. The system of equations is represented graphically in Fig. S7 – in Fig. S7a with the annual change factors; in Fig. S7b, these are transformed into percentage change rates for convenience of the further description. The two left-hand columns and the upper three rows show the annual change rates as applied in Fig. S6. The grey cells indicate the variable composition per row by multiplication of the indicated variables per column; for example, the annual energy consumption change factor (1.021) is supposed to be equal to the product of the change factors for population (1.014) and energy consumption per capita (1.0069), the product written into the rightmost column. The condition is that the product (rightmost column) matches the value from the graphs (second left column), which is shown to be fulfilled for the entire equation system.

The results are summarized as follows: 3.4 %/year GDP growth is composed of growth per capita by 2 %/year and population by 1.4 %/year. 2.1 %/year of the GDP growth are energy relevant, as energy consumption decreases by 1.28 %/year per unit of GDP. The 2.1 %/year is the CO_2 emissions growth if emissions per unit of energy consumption remain constant over time, while CO_2 emissions per unit of energy consumption shrink by 0.4 %/year. Bottom line, GDP growth leads to 1.7 %/year rise in CO_2 emissions. In the main article, an effective emissions reduction of at least 2 %/year is inferred requested, which means a required emissions reduction of 3.7 %/year relative to unchanged GDP growth. From subjective general experience, reduction of 3 %/year by the widely discussed abatement measures (see main article with further references) seems feasible yet ambitious, 2 %/year rather realistic. Thus, it appears indispensable that current GDP growth be narrowed towards zero.

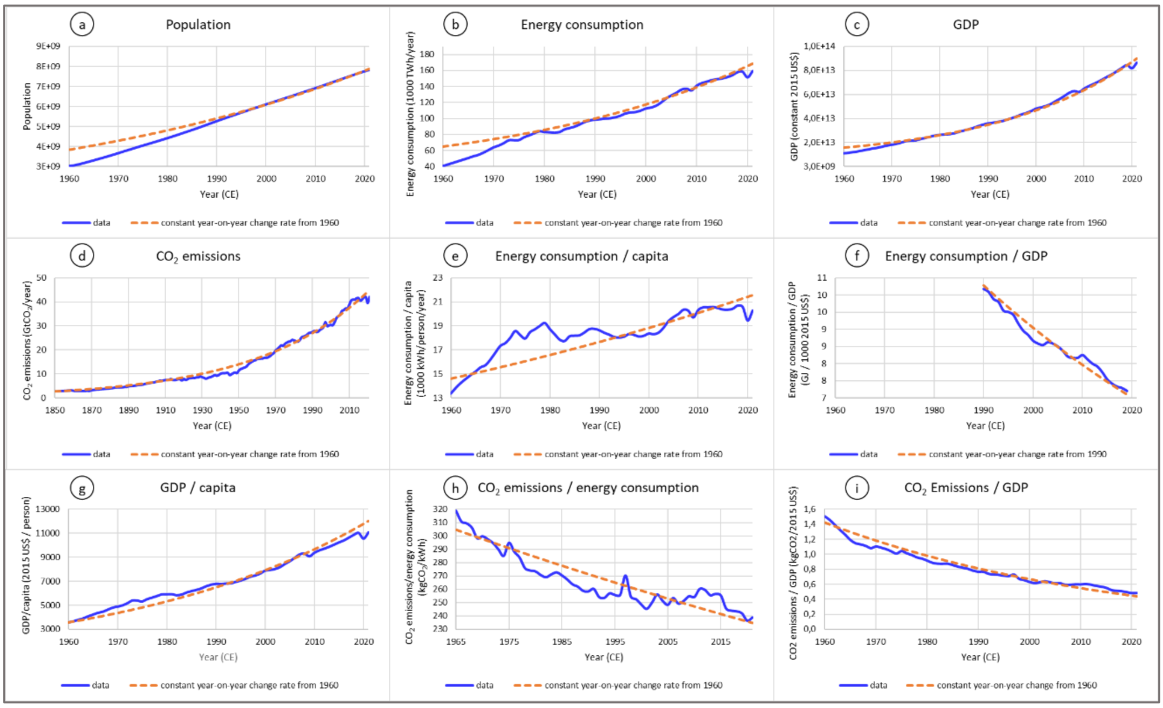

Fig. S6. Published data (solid blue lines) and exponential (geometric) trends with constant annual change rates each (dashed orange lines). (a) Population [69]; (b) energy consumption [70]; (c) global gross domestic product, GDP [71]; (d) CO_2 emissions [72, 73]; (e) energy consumption per capita, published data shown as [70]/[69] (values of [70] divided by values of [69]; (f) energy consumption per unit of GDP [74]; (g) GDP per capita, [71]/[69]; (h) CO_2 emissions per unit of energy consumption, ([72]+[73])/[70]; (i) CO_2 emissions per unit of GDP, ([72]+[73])/[71].

Alternatively, additional emissions caused by economic growth may be covered by carbon capture and utilization/storage (CCUS). The cost-neutral reduction by 90 % of the total present emissions, as previously inferred [8], has been estimated without the costly, partly environmentally risky, and juvenile CCUS; CCUS is required to tackle the residual 10 % of persistent emissions. If CCUS is to additionally allow for economic growth, a brief potential/cost analysis is summarized in the following lines for the case of 2 %/year emissions reduction (year on year from present emissions), 3.43 %/year GDP growth (year-on-year into the future), related 1.65 %/year CO_2 emissions growth, and CCS to capture the growth-induced emissions.

Related to CCS cost by order of magnitude (for capture, transport, and storage), the present estimates are based on – presumably representative – 100 $/t$CO_2$, linearly approaching 50 $/t$CO_2$ by 2050, and remaining constant afterwards. Related to carbon removal quantities of CCS (CCU perhaps adding 10 % of CCS), the storage potential has been estimated to 1,525 GtCO_2 for USA, Europe, and China combined (page 125 of [75]). In an earlier study for the world, the storage potential was estimated to approximately 1,660 GtCO_2 [76]. To capture the additional emissions from economic growth (1.65 %/year rise beyond those of the 2 %/year emissions reduction) by CCS, (i) the storage capacity will be exhausted by year 2099 and 2082 for the USA/Europe/China and world estimates, respectively; (ii) as example for Europe, CCS would annually cost approximately 0.18 % of GDP throughout (most of) this century, for the world about 0.46 % of GDP (details in supplementary data and code).

			Energy consumption			CO_2 emissions		
a		Population	per capita	per GDP	GDP/capita	per en. cons.	per GDP	Multiplication
	Graph	1,014	1,0069	0,987	1,020	0,996	0,983	
Population	1,014							
Energy consumption	1,021							1,021
	1,021							1,021
CO_2 emissions	1,0165							1,0165
	1,0165							1,0165
GDP	1,0343							1,0343
GDP per capita	1,02							

			Energy consumption			CO_2 emissions		
b		Population	per capita	per GDP	GDP/capita	per en. cons.	per GDP	Multiplication
	Graph	1,40%	0,69%	-1,28%	2,00%	-0,44%	-1,72%	
Population	1,40%							
Energy consumption	2,10%							2,10%
	2,10%							2,10%
CO_2 emissions	1,65%							1,65%
	1,65%							1,65%
GDP	3,43%							3,43%
GDP per capita	2,00%							

Fig. S7. Graphical representation of the multi-equation system for the annual change rates of population, energy consumption, GDP, CO_2 emissions, and derivatives. (a) copied into (b) with annual change factors translated into percentual change fractions. (a) Left two columns and first three rows: variables and their values as of Fig. S6 (dashed orange lines); variables in the left column comprehended composed by multiplying the grey-associated variables of the first two rows (e.g., annual change factor for energy consumption equal product of annual change factors for population and energy consumption per capita), the result of the product given in the right-most column, fulfilling the condition of equality to the values given by the graphs of Fig. S6, here listed in the second-left column.

Regarding marginal cost versus removal potential, the industrial sectors have previously been examined for Sweden and the Netherlands [77, 78]. As a result, CCS can reach approximately half of the emissions at approximately 80 Euro/tCO_2, with larger coverage possible at higher costs. Worldwide, for comparison, industry contributes 26 % to total CO_2 emissions (based on [5]); a 50 % CCS-reach (at reasonable cost) would correspond to 13 % of total emissions.

S8. Cost from future sea level rise

The present estimation of cost from sea level rise is based on a practical framework. Herein, the total cost is composed of (i) annual adaptation investment and residual damage (DAMAGE), (ii) land abandonment (ABANDON).

The costs of residual damage and land abandonment are viewed as proportional to the asset values at stake. Asset values appear to develop linearly with GDP, 2.8 as the proportionality factor in [29] based on the data of [79]. Within the latter data, the sum of produced and natural capital seems to exhibit a proportionality factor of 3.2 between GDP and capital. In summary, a factor of 3 is viewed as a useful rule of thumb (as customs, both GDP and capital considered in monetary units).

GDP is given by population and GDP/capita. Hence, for a certain sea level and population, damage from sea level rise is proportional to GDP/capita; and for constant sea level and GDP/capita, damage is proportional to population. Furthermore, for a given population and GDP/capita (i.e., given GDP), damage is assumed to be roughly proportional to sea level rise. In fact, this relationship turns out to hold well for spatial aggregations (e.g., at global and regional level) and at the town level perhaps for elevated sea levels beyond the order of 1 m above the present (see study 3 below). In short, Damage ~ SeaLevelRise · GDP = SeaLevelRise · Population · GDP/capita, or Damage/SeaLevelRise/GDP an environment-specific constant. This applies to non-altering socioeconomic conditions and needs to be adapted if environmental specifics change over time. This simple framework is used for projections based on the data of three previous studies, the results presented next.

(1) The present population vulnerable to sea level rise has been published per country and for the world pursuing two approaches, CoastalDEM and SRTM; vulnerable is defined as living below Mean Higher-High Water [31]. CoastalDEM exhibits 2-4 times the vulnerability of SRTM. The description of the present analysis focuses on the newer and more sophisticated CoastalDEM results. Of these data, the global vulnerable population is depicted on the left-hand side of Fig. S8 for sea levels up to 5 m higher than today, the dotted straight lines inserted to verify the proportionality of the vulnerable population to sea level rise.

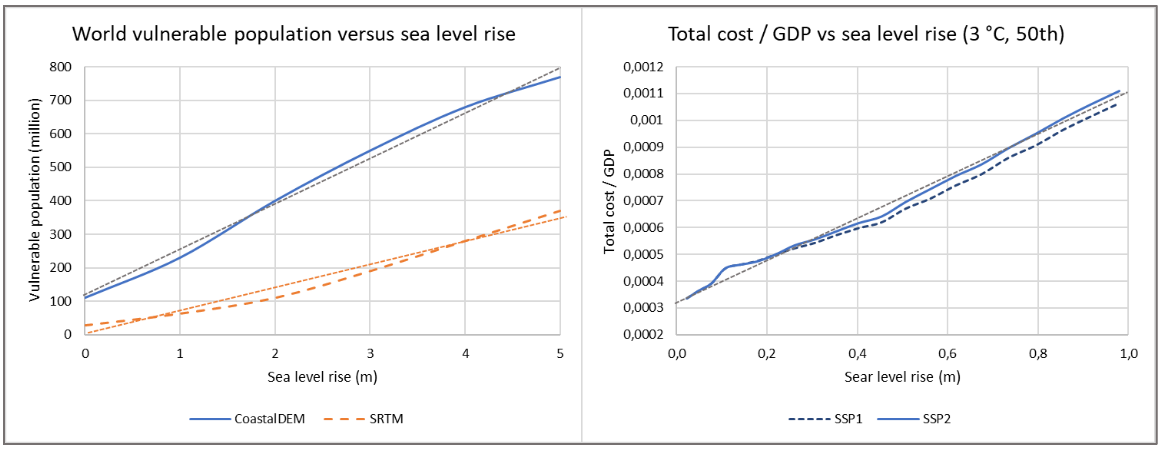

Fig. S8. Left: Global vulnerable population per sea level rise for CoastalDEM and SRTM, data of [31]. Right: Total cost caused by sea level rise (here adaptation plus residual damage) per unit of GDP versus sea level rise for the socioeconomic scenarios SSP1 and SSP2, data of [30]. Dotted straight lines to guide the eye.

The present framework is transformed to the vulnerability data as Damage ~ SeaLevelRise · VulnerablePopulation/SeaLevelRise · GDP/capita, with VulnerablePopulation/SeaLevelRise the proportionality constant in VulnerablePopulation ~ SeaLevelRise (Fig. S8, left), GDP/capita an indication of wealth per person, VulnerablePopulation · GDP/capita an indication for the asset values exposed to regular damage. For losses from land/asset abandonment (Abandon), the same relationship is used, with the difference that VulnerablePopulation relates to the abandoned land. The land is counted as abandoned after 2 m of further sea level rise. For instance, in finite steps, once sea level rise reaches 3 m, the vulnerable population related to 1 m sea level rise is an indicator of abandoned assets. The total cost is the aggregate Damage + Abandon.

This framework is applied to the CoastalDEM vulnerable population data interpolated for the sea level projection of the current work, as shown by the dashed blue line in Fig. S4. Here, by round figures, 1 m sea level steps are reached by the years 2100, 2400, 2600, 2900, and 3100 from 1 to 5 m above the preindustrial level. For a translation into economic impact, the vulnerable population is scaled with current flood loss data, i.e., 0.1 m sea level rise since 2000 (CoastalDEM data relating to zero sea level rise in 2000), interpolated to 122 million vulnerable persons (110 million in 2000 with zero sea level rise); US$ 90 billion global damage from floods [80], times 2/3 for coastal flood fraction, times 3/2 to include adaptation cost (the latter here for simplicity, a factor of 2 possible, see below); US$ 96,100 billion as global GDP. These figures relate to present global coastal flood damage (including adaptation cost) of about 0.1 % of GDP with 2 % of world population vulnerable. This relationship allows to readily scale any other sea level rise-affected population under the present conditions. Thus scaled, 5 m sea level rise correspond to a global annual damage of 0.6 % of GDP (GDP related to the area at risk). As inferred above, this cost given in the fraction of GDP will be constant over time for the specific sea level rise of 5 m and constant socioeconomic conditions, which will finally be reached by year 3100 according to the present estimation.

Further analysis accounts for the following socioeconomic changes in the future: population growth until year 2100 by 40 %, twice in coastal vicinity, constant population afterwards; the coastal asset values twice the country averages; settlement retreat as precedingly described, at least constant asset at risk after retreat as probable result of continued small-scale relocation; division by fraction of non-vulnerable to total population, cap at 100 % of GDP, inversely reflecting drowned land probability, cost of 100 % GDP corresponding to drowned country. With these figures, total cost from sea level rise of 5 m above the preindustrial level by year 3100 is indicated as 1.2 % of GDP on global average. At country level, 17 countries (out of 175) are affected by more than 10 % of GDP, representing 4 % of the total world population and 1.9 % of the global GDP. Severely endangered countries are Bahamas, Cayman Islands, Kiribati, Maldives, Marshall Islands, Suriname, Tuvalu (>80 % of GDP) with 0.019 % of total world population and 0.017 % of global GDP; Bahrein, Guyana (40-70 % of GDP); Bangladesh, French Guiana, Netherlands, Northern Mariana Islands, Tonga, Turks and Caicos Islands, United Arab Emirates, Vietnam (10-30 % of GDP). Most of these countries exhibit GDP/capita below 10,000 US$; larger GDP/capita are in Bahamas, Bahrein, Northern Mariana Islands, Turks and Caicos Islands, United Arab Emirates (20,000-40,000 US$), and in the Netherlands as well as the Cayman Islands (50,000-100,000 US$). For comparison, the original vulnerable population data reveal the following countries with a present ratio of vulnerable to total population above 50 % for 5 m sea level rise: Maldives (100 %), Cayman Islands (98 %), Kiribati (95 %), Marshall Islands (94 %), Tuvalu (90 %), Bahamas (87 %), Suriname (86 %), Bahrein (78 %), Guyana (78 %), Turks and Caicos Islands (75 %), Netherlands (71 %), United Arab Emirates (66 %), Tonga (60 %), Vietnam (59 %), French Guiana (55 %), Bangladesh (51 %) [31].

From the present estimation framework, global cost from abandonment (asset loss) is negligible until year 2100, peaks by year 2600 at 35 % of damage (including abatement), and vanishes again towards year 3100.

(2) A further previous study also supports a proportionality assumption of the present framework [30]. The right-hand side of Fig. S8 shows the total cost from sea level rise (total cost here from adaptation plus residual damage) per unit of GDP in dependence on sea level rise for the case of 3 °C warming since preindustrial times until the end of this century (50^{th}

uncertainty percentile) and for the socioeconomic cases SSP1 and SSP2. Clearly, the total cost per GDP is exhibited as proportional to sea level rise.

Further characteristics of the previously used data are summarized in Fig. S9. The data are differentiated by country income group, temperature scenario, sea level, and socioeconomics. Climate conditions range from *<1.5 °C* to *4 °C* temperature by year 2100 (italics for scenario notation, presumed self-explaining); entailed sea level rise is given for the *5th*, *50th*, and *95th* percentiles of uncertainty range; socioeconomic scenarios are *SSP1* through *SSP5*; regarding country income groups, the present description concentrates on all income groups (global) as well as differentiating between *low* and *high (OECD)* income groups.

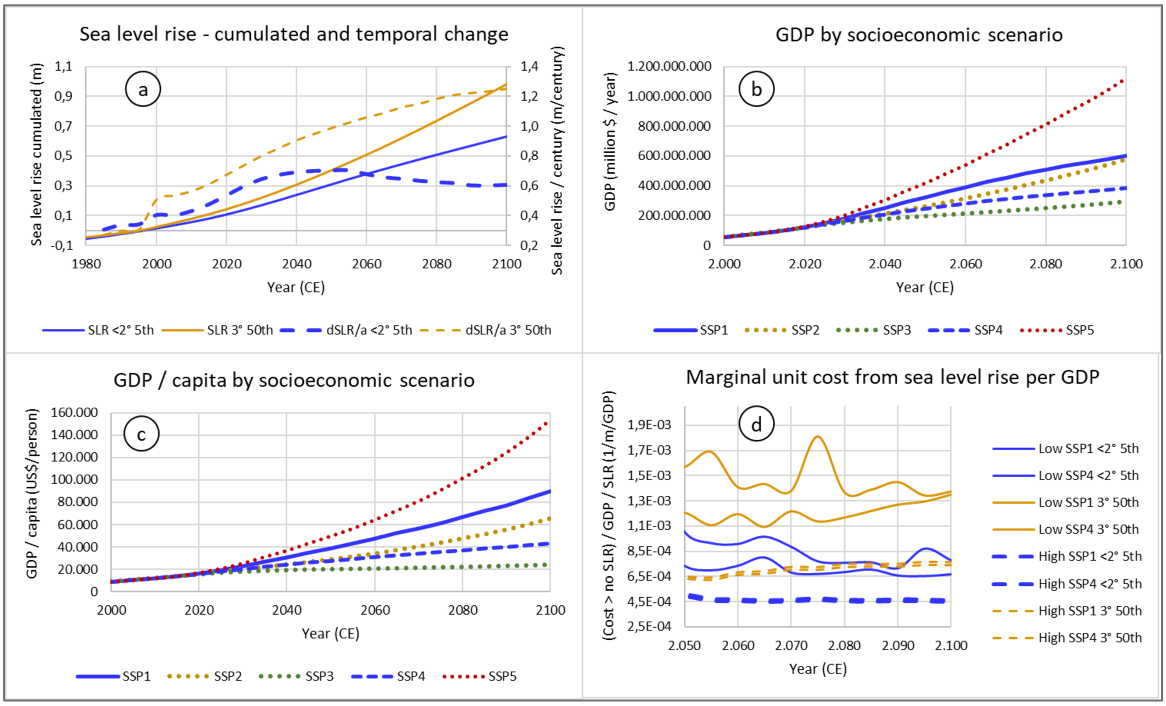

Fig. S9. Graphics to selected data of [30]. (a) Sea level rise (SLR) (solid lines, left vertical scale) and translated into velocity (dashed, right vertical scale) for two temperature projections until the end of the century, *<2 °C* (blue) and *3 °C* (brown) at the *5th* and *50th* uncertainty percentiles, respectively. (b) GDP for the five socioeconomic scenarios. (c) GDP/capita from GDP and population. (d) Marginal cost (total cost at a certain sea level rise minus total cost at sea level rise zero; total cost equal abatement cost plus residual damage) divided by GDP and divided by sea level rise for *low* (solid) and *high-OECD* (dashed) income groups, for the scenarios *SSP1,<2 °C,5th* (blue) and *SSP4,3 °C,50th* (brown).

Fig. S9a shows the data for the expected sea level rise from the present (in meters; solid lines, left scale) and transformation into rise velocity (meters/century; dashed lines, right scale) for the cases *<2 °C 5th* and *3 °C 50th*. The former scenario exhibits a (more or less) constant velocity in the future in the order 0.6 m/century. As this is close to the velocity derived above (0.4-0.5 m/century), the corresponding results of [30] are preferred for the present analysis. As a sensitivity indication, Fig. S9a also contains the data for the *3 °C 50th* scenario with continuous acceleration of sea level rise (brown dashed line).

Fig. S9b-c show the data for GDP and GDP/capita for various socioeconomic scenarios. SSP5 (red dotted) is viewed as extreme and disregarded in the further consideration for conciseness reasons. SSP1 is next in GDP growth and is therefore used for the present analysis (average annual growth rate 2.4 %/year, year on year). From figure 5 in [30] (total cost as a fraction of GDP), the income groups *low* and *high (OECD)* seem to form the boundaries, first regarding absolute levels of cost/GDP (*high income (OECD)* at the low boundary), and second regarding the change from year 2050 to 2100 (*low income* with large change for *SSP1*); thus, these two income groups are presently considered further, denoted by *high* and *low*. *SSP4* exhibits the largest GDP-growth for *low* income with 3.4 %/year, hence also regarded here.

The marginal total cost is the total cost for a certain sea level rise subtracted by the corresponding total cost for zero-sea level rise. In Fig. S9d, the marginal cost is divided by sea level rise and again divided by GDP; the blue lines refer to *<2 °C* 5^{th}, solid for *low* income and dashed for *high* income. Apparently to the first order, the underlying data consider cost per unit of sea level rise proportional to GDP or vice versa, cost per unit of GDP proportional to sea level rise. The same can be inferred for the *3 °C* case, albeit with a larger spread (brown lines).

For further insight, the marginal costs per unit of sea level rise are approximately on average combined for SSP1 and SSP4:

- *<2 °C*, 5^{th}-50^{th}-95^{th} percentile: 0.072-0.098-0.13 and 0.045-0.06-0.074 (% of GDP)/m for *low-income* and *high-income* countries, respectively.
- *3 °C*, 5^{th}-50^{th}-95^{th} percentile: 0.098-0.13-0.18 and 0.06-0.075-0.093 (% of GDP)/m for *low-income* and *high-income* countries, respectively.

Because the sea level rise of *<2 °C* 5^{th} applies best to the present analysis (see above), the values 0.072 and 0.045 (% of GDP)/m are used for *low*- and *high-income* countries, respectively, when scaling to the expected 5-6 m of sea level rise in approximately 1,100 years.

(3) In a further previous study, the flood exposure of the largest 136 coastal towns was examined for sea level rises from the present (year 2005) by 10, 20, and 30 cm, associated with the years 2030, 2050, and 2070, respectively [29]. For the present work, exemplary results have been analysed in further detail with the following outcomes. First, the data exhibit proportionality of flood damage to GDP for a constant present sea level, supporting a major assumption of the present framework.

Second, marginal damage per unit of GDP and per unit of sea level rise (here termed ‘specific damage’) appears to increase with sea level rise. An instance of the pattern is: specific damage rising by a factor of 2 from 10 to 20 cm sea level rise and by a factor of 1.75 from 20 to 30 cm sea level rise. This is applied to an example of the published data (Model 1, socio-economic scenario with no city limit, optimistic sea level rise with subsidence, file ‘(No1) Opt_SLR_NL_SEC_Results.xls’) for a sea level rise of 5 m, and the damage expressed as a percentage of GDP including a factor of 2 to account for adaptation cost in the same order as damage cost [29]. The following towns emerge with flood costs higher than 70 % of GDP: Hai Phòng (Vietnam), Abidjan (Ivory Coast, Gulf of Guinea), Khulna (Bangladesh), Guayaquil (Ecuador), Thành-Pho-Ho-Chí-Minh (Vietnam). The following towns are attributed to 20-70 % flood cost of GDP: Lagos (Nigeria), Maputo (Mozambique), New Orleans (USA), Conakry (Guinea), Virginia Beach (USA). It should be noted that a view to the elevation of Abidjan reduces the precedingly derived severity.

S9. Climate-related economic losses apart from sea level rise

Climate-related cost has previously been differentiated by the sectors of coastal and low-lying settlements (related to floods and storms), agriculture (with forestry and fisheries), water supply, human health, natural ecosystems, and infrastructure [27]. In the preceding chapter, the cost of the first sector has been examined, i.e., related to sea level rise. In the present work, instead of analysing the costs by sector, the further costs are examined by cause.

For the USA, data are available for the causes of freeze, wildfire, winter storm; storm, flood, drought; and tropical cyclone/hurricane [81]. The cost contributions of the first three are revealed negligible; those of the second three exhibit no frequency change with the temperature increase during the past decades for damages per year greater than 0.2 % of GDP. The latter damages, i.e., from tropical cyclones, amount to about 50 % of all climate-related losses and appear to have strengthened with rising surface temperatures. Hence, losses from tropical cyclones are considered as the driving term of the climate-related damages besides losses from sea level rise.

On average for the period 1984-2014, damages from tropical cyclones amounted to 0.15 % of GDP in the USA, in the order of 0.11 % of GDP in China, and 0.06 % of GDP worldwide, based on the data of [81, 82, 83], respectively. During the same period, the average temperature was 0.7 °C above preindustrial levels. The economic losses have risen linearly with temperature by 0.5 % of GDP per 1 °C of warming in the USA [81] and by 0.19 %/°C worldwide [83]. Losses from the other causes than from tropical cyclones are revealed uncorrelated with surface temperature for the USA [81] and inversely correlated for the EU (in the EU, tropical cyclone impact assumed negligible) [84, 85].

For projections, the influence of rising surface temperatures on the climate-related damaging events is a fundamental input. First looking into the past for the driving term, i.e., the tropical cyclones, regional strengths have developed linear with surface temperature, proportional in the North Atlantic and inverse proportional in the Eastern North Pacific, measured as the aggregate of storm intensity, frequency, and duration by the Power Dissipation Index, PDI [86]. Second looking into the future, previous sophisticated simulations predict PDI proportional to surface temperature for the temperature range considered by the present work (i.e., up to 2.1 °C warming relative to preindustrial times, see Fig. 1 of the main article) when comparing the simulation results of [87] with the corresponding temperatures of [88].

For completeness of the present description, precipitation of tropical cyclones has previously been predicted to increase by 7 % per 1 °C of warming [89]. According to paragraph S4 above, heavy precipitation events have strengthened by 3-6 % per decade, which translates into 17-33 %/°C related to surface temperature change. Hence, this can be decomposed into 7 %/°C for tropical cyclones and 10-26 %/°C for all other causes.

In summary, tropical cyclones represent the driving term in climate-related economic losses regarding quantity and temperature dependency. At present, the related global losses amount to 50 % of total losses, per year to roughly 0.1 % of GDP at an industrial-age warming of 0.7 °C, and will reach 0.4 % of GDP with a warming of 2.1 °C (which is the peak at 2 %/year carbon emissions reduction, cf. figure 2 of the main article). Due to the lack of further detailed knowledge, the losses from the other causes than sea level rise are assumed to be twice those from the tropical cyclones to first order, thus 0.2 % of GDP at present and 0.8 % of GDP at 2.1 °C on global average.

S10. Complementary notes

Anthropogenic attribution

For conciseness reasons, the present description bypasses the topic of anthropogenic attribution, that is, the impact of humankind in addition to the natural processes. The present view is briefly summarized for completeness.

To the very first order, 'left-alone' nature is regarded balanced. A good example may be terrestrial vegetation; as much CO_2 is taken from the atmosphere to have a tree grow, as much is released after its death. It appears highly important to have this first-order understanding spread more widely, because it is required for a solid common knowledge base within broader society. Next, it is important to know that volcanoes have no significant influence on the atmospheric CO_2 budget (during the present geological eon).

Within society, there is supposedly no argument against anthropogenic carbon being released into the air. As the CO_2 concentration in the atmosphere is observed to increase, and the origin is not (sufficiently) explainable by natural processes, the human emissions must be recognized as the cause of rising atmospheric CO_2 concentrations. Next, we understand that nature removes some part of these entries from the atmosphere into the oceans and the terrestrial vegetation. Bottom line, the observed CO_2 increase reflects the human emissions minus the natural removal.

To understand the influence of the atmospheric CO_2 concentration on the climate, the present approach starts with the following hypothesis. If CO_2 is as important for the climate as is commonly communicated, it must show a clear fingerprint through nature's past. Indeed, going back through 400 million years, the observations strongly support a very simple function for the temperature contribution of CO_2 [1].

In summary, anthropogenic attributions to climate change appear unequivocal. If there is still doubt, the risk must be assumed that the present (and commonly communicated) explanation of nature is correct. Consequently, humankind is obliged to act accordingly.

Feedback mechanisms

The present description of nature makes no explicit mention of the term 'feedback mechanism'. Here, feedback mechanisms are considered as intrinsic properties that either deserve distinct insight or are a seamless part of the functioning of nature.

Related to the former, the driving components are addressed in the present description. Prominent examples include amplification of the CO_2-temperature effect by water vapor (H_2O); amplification of the temperature impact from CO_2 (and entailed H_2O) by temperature-driven effects, particularly due to (snow/ice) albedo change; dynamic vegetational CO_2 uptake on land in dependence on the atmospheric CO_2 concentration and the surface temperature; and ocean heat uptake diluting the CO_2 and H_2O radiative effect on the (mean global annual) surface temperature in an asymptotic manner for about a millennium.

Related to the seamless components of the natural processes, these are examined in separate detailed descriptions. Examples include lapse rate change with surface temperature; areas of warming and cooling vertically distributed in the atmosphere depending on the surface temperature as well as the CO_2 and H_2O concentrations; and the adaptation of clouds to surface temperature within Earth's energy balancing mechanisms [3].

Cooling from aerosols

The recognized cooling effect from aerosols, particularly sulphur-based, is disregarded in the present description.

The natural contributions are presumed to be included in the Eocene relationship because this is derived from observations before an anthropogenic influence.

The anthropogenic contributions are assumed to play a minor role and/or to be cancelled out by other effects not considered in the present description. Interestingly, anthropogenic sulphuric entries into the atmosphere may shrink as carbon emissions decrease, thus reducing the cooling contribution with the intended transition to low/zero carbon.

Social discount rates and intergenerational ethics

The present description bypasses the discussions on the social discount rates and ethics. The social discount rate can be considered as a parameter to value ethical aspects. The present work presumes carbon emissions reductions of at least 2 %/year; lower emissions reduction is called irresponsible. The social discount rate attempts to quantify such 'irresponsibility' in economic terms and on this base, to support cost/benefit quantification of potential measures.

Additional notes on ethical aspects start with a sketch of key social developments looking from the past through the present into the future. In the past, generations not only have brought the burden of climate change to the future generations but also have created long-lasting benefits enabled by the utilization of fossil carbon (e.g., progress in medicine and pharmacy facilitated by low-cost energy); the population development followed the given possibilities accompanied by significant exploitation of natural resources in general (e.g., regarding nutrition and heating). The present generation needs to reverse carbon emissions, performable at low cost; damage from climate change has set in at local level, frequently at locations different from those of past emissions (e.g., regarding areas of glacier melting, droughts, heavy rain events) and in far distance to benefit from the past achievements (e.g., regarding medicine and energy generation technology); population is growing; orientation is largely towards growing welfare, exploitation of the natural resources is continuing (through changing resource types), required recycling not yet sizably contributing to resource supply. Future generations must base wealth (welfare) increase on energy from renewables; they need to adapt to climate change impact (particularly from sea level rise and temperature increase) and resources availability (e.g., regarding potential resources exhaustion); climate adaptation cost and residual damage can remain at bearable levels; population development will resume to orient itself towards the possibilities to live (e.g., regarding the availability of resources).

The preceding sketch raises the following thoughts. First, it is obvious that those uninvolved in the causes of climate change need support by the international community to reduce the harm-benefit imbalance; developing countries need also support to base energy supply on renewables (e.g., through knowledge transfer and implementation of the related industry). Second, the expected changes will continuously bear inequalities due to the regional inhomogeneity. Third, in case the global population will downsize, the process will inherently be accompanied by human suffering; a major cause will probably lie in Earth's limited capacity to support human population.

In conclusion, the preceding frame renders economic and ethical considerations quite complex, more complex than typically incorporated in the discussions. A thorough analysis is beyond the present scope.

Geoengineering

Geoengineering has been disregarded in the present work. The arguments, pro and contra, can be found in the available literature. At this point, to re-emphasize the described sine qua non-actions: They are considered indispensably required near-term. Second, geoengineering resembles business-as-usual in terms of continuing technical exploitation of nature's potentials; it appears doubtful whether geoengineering can meet ethical standards.

Covid, war, and supply chain disruption starting in 2020

For continuity of the descriptions, the economic disruptions and the entailed CO_2 emissions variability since 2020 are disregarded in the present article. If perceived as required for detailed insight and projections, the parameters of the present study need to be adapted in a separate work.

Economic growth and emissions mitigation

In the present work, detailed considerations are presented on the impact of economic growth on the fate of mitigation attempts.

For the broader public, the following illustration may be of additional help.

As an example of private life, let us imagine replacing our existing car with another vehicle that consumes half gasoline per mileage. As the new car comes into operation, we decide to drive twice. Consequently, gasoline consumption remains constant.

This example reveals the importance of separating consumption reduction through equipment replacement from equipment usage. Translated to the transition towards low/zero carbon emissions, there is remarkable potential to reduce emissions by equipment (and process) replacement. Realistically, this transition is time consuming. Therefore, the reduction by equipment replacement is viewed via the implementation pace, that is, the realized emissions reduction per year. If the entire equipment portfolio is used more frequently than before, which is the case in the tail of economic growth, this counteracts the annual emissions reduction from equipment replacement.

For completeness, a slight numerical deviation is mentioned related to the pursued considerations. Assuming equipment replacement by 2 % in a year and utilizing the residual 98 % of the previous equipment 2 % more often, the utilization of the previous equipment amounts to $0.98 \cdot 1.02 = 0.9996$. In the present context, this means an emissions reduction of 0.04 %/year.

Data accessibility: Data and code are provided as separate file.

References

1. Anderl, T. (2021). The climate role of CO_2 – nature's telling from 400 Mio. years. *Research Square*, preprint. doi: 10.21203/rs.3.rs-524780/v1. pdf: The climate role of CO2 – nature's telling from 400 Mio. years - pdf.
2. Anderl, T. (2022). The climate roles of H_2O and CO_2 from longwave absorption. *Research Square*, preprint. doi: 10.21203/rs.3.rs-830246/v1. pdf: The climate roles of H2O and CO2 from longwave absorption - pdf.
3. Anderl, T. (2021). Planetary emittance and feedback parameters through varying climates in basic modelling. *Research Square*, preprint. doi: 10.21203/rs.3.rs-692319/v1. pdf: Planetary emittance and feedback parameters - pdf.
4. Anderl, T. (2021). Earth's balanced climates in view of their energy budgets. *Research Square*, preprint. doi: 10.21203/rs.3.rs-568771/v1. pdf: Earth's balanced climates in view of their energy budgets - pdf.
5. Anderl, T. (2021). CO_2 emissions and climate - nature's prospect on Green Growth. *Research Square*, preprint. doi: 10.21203/rs.3.rs-547822/v1. pdf: Nature's prospect on Green Growth - pdf.
6. Anderl, T. (2022). Climate change into reverse gear – reversibility and legacies. *Research Square*, preprint. doi: 10.21203/rs.3.rs-1652932/v1. pdf: Climate change - reversibility and legacies - pdf.
7. Anderl, T. (2022). The role of land use in climate change. *OSF Preprints*. doi: 10.31219/osf.io/zg8n7.
8. Anderl, T. (2022). CO_2 abatement economics - a practical view. *Research Square*, preprint. doi: 10.21203/rs.3.rs-1187536/v1. pdf: CO2 abatement economics - a practical view - pdf.
9. Myhre, G., Highwood, E. J., Shine, K. P., & Stordal, F. (1998). New estimates of radiative forcing due to well mixed greenhouse gases. *Geophysical Research Letters*, **25**, 14, 2715-2718. doi: 10.1029/98GL01908.
10. Bond-Lamberty, B., & Thomson, A. (2010). Temperature-associated increases in the global soil respiration record. *Nature*, **464**, 579–582. doi: 10.1038/nature08930.
11. Zhou, T., Shi, P., Hui, D., & Luo, Y. (2009). Global pattern of temperature sensitivity of soil heterotrophic respiration (Q 10) and its implications for carbon-climate feedback. *J. Geophys. Res.*, **114**, G02016. doi:10.1029/2008JG000850.
12. Wu, C., Liang, N., Sha, L., Xu, X., Zhang, Y., Lu, H., et al. (2016). Heterotrophic respiration does not acclimate to continuous warming in a subtropical forest. *Sci Rep*, **6**, 21561. doi: 10.1038/srep21561.
13. Schimel, D., Stephens, B. B., & Fisher, J.B. (2015). Effect of increasing CO_2 on the terrestrial carbon cycle. *Proc Natl Acad Sci USA*, **112** (2) 436-441. doi: 10.1073/pnas.1407302112.
14. MacDougall, A. H., Frölicher, T. L., Jones, C. D., Rogelj, J., Matthews, H. D., et al. (2020). Is there warming in the pipeline? A multi-model analysis of the Zero Emissions Commitment from CO_2. *Biogeosciences*. **17**, 2987-3016. doi: 10.5194/bg-17-2987-2020.

15. Paprotny, D., Sebastian, A., Morales-Nápoles, O., & Jonkman, S. N. (2018). Trends in flood losses in Europe over the past 150 years. *Nat Commun*, **9**, 1985. 10.1038/s41467-018-04253-1.

16. Blöschl, G., Kiss, A., Viglione, A., Barriendos, M., Böhm, O., Brázdil, R., et al. (2020). Current European flood-rich period exceptional compared with past 500 years. *Nature*, **583**, 560–566. 10.1038/s41586-020-2478-3.

17. McKay, D. I. A., Staal, A., Abrams, J. F., Winkelmann, R., Sakschewski, B., Loriani, S., et al. (2022). Exceeding 1.5°C global warming could trigger multiple climate tipping points. *Science*, **377**, 6611, p. 1135. doi: DOI: 10.1126/science.abn7950.

18. Rothman. D. H. (2017). Thresholds of catastrophe in the Earth system. *Sci. Adv.*, **3**, 9: e1700906. doi: 10.1126/sciadv.1700906.

19. Ritchie, H., Roser, M., & Rosado, P. (2020). CO_2 and Greenhouse Gas Emissions. *OurWorldInData.org*. Data retrieved from https://ourworldindata.org/co2-emissions, before 26 October 2022.

20. Net zero emissions race. (2022). *Energy & climate intelligence unit*. Online resource, https://eciu.net/netzerotracker. Data retrieved from https://zerotracker.net/, 20 December 2022.

21. Deng, Y., Cornelissen, S., Klaus, S., Blok, K., van der Leun, K., Worrell, E., et al. (2011). The ECOFYS energy scenario. In: The Energy Report. 100% Renewable Energy by 2050 [Singer S, Denruyter JP (eds.)] *WWF International, Gland (Switzerland)*. Accessed from The Energy Report. 100% Renewable Energy by 2050.

22. IRENA. (2022). Urban energy transition for the Greater Metropolitan Area of the Central Valley of Costa Rica, International Renewable Energy Agency, Abu Dhabi.

23. Agajelu, B. O., Ekwueme, O. G., Obuka, N. S. P., & Ikwu, G. O. R. (2013). Life Cycle Cost Analysis of a Diesel/Photovoltaic Hybrid Power Generating System. *Industrial Engineering Letters*, **3**, 1, 19-30. www.iiste.org.

24. Lozano, L., Querikiol, E. M., Abundo, M. L. S., & Bellotindos, L. M. (2019). Techno-economic analysis of a cost-effective power generation system for off-grid island communities: A case study of Gilutongan Island, Cordova, Cebu, Philippines. *Renewable Energy*, **140**, 905-911. https://doi.org/10.1016/j.renene.2019.03.124.

25. Katsivelakis, M., Bargiotas, D., Daskalopulu, A., Panapakidis, I. P., & Tsoukalas, L. (2021). Techno-Economic Analysis of a Stand-Alone Hybrid System: Application in Donoussa Island, Greece. *Energies*, **14**, 1868. https://doi.org/10.3390/en14071868.

26. Katsoulakos, N. M. (2019). An Overview of the Greek Islands' Autonomous Electrical Systems: Proposals for a Sustainable Energy Future. *Smart Grid and Renewable Energy*, **10**, 55-82. https://doi.org/10.4236/sgre.2019.104005.

27. Parry, M., Arnell, N., Berry, P., Dodman, D., Fankhauser, S., Hope, C., et al. (2009). Assessing the Costs of Adaptation to Climate Change: A Review of the UNFCCC and Other Recent Estimates. *International Institute for Environment and Development and Grantham Institute for Climate Change, London*. https://www.iied.org.

28. Buchner, B., Naran, B., Fernandes, P., Padmanabhi, R., Rosane, P., Solomon, M., et al. (2021). Global Landscape of Climate Finance 2021. *Climate Policy Initiative*. https://www.climatepolicyinitiative.org.

29. Hallegatte, S., Green, C., Nicholls, R., & Corfee-Morlot, J. (2013). Future flood losses in major coastal cities. *Nature Clim Change* **3**, 802-806. doi: 10.1038/nclimate1979. 10.1038/nclimate1979.

30. Brown, S., Jenkins, K., Goodwin, P., Lincke, D., Vafeidis, A. T., Tol, R. S. J., et al. (2021). Global costs of protecting against sea-level rise at 1.5 to 4.0 °C. *Climatic Change*, **167**, 4. doi: 10.1007/s10584-021-03130-z.

31. Kulp, S. A., & Strauss, B. H. (2019). New elevation data triple estimates of global vulnerability to sea-level rise and coastal flooding. *Nat Commun* **10**, 4844. doi: 10.1038/s41467-019-12808-z.

32. Nordhaus, W. (2015). Climate Clubs: Overcoming Free-riding in International Climate Policy. *American Economic Review*, **105** (4): 1339–1370. doi: 10.1257/aer.15000001.

33. Spratt, R. M., & Lisiecki, L. E. (2016). A Late Pleistocene sea level stack. *Clim. Past* **12**, 1079–1092. doi: 10.5194/cp-12-1079-2016. Data retrieved from https://www.sealevels.org/, 2022-03-15.

34. Kopp, R. E., Kemp, A. C., Bittermann, K., Horton, B. P., Donnelly, J. P., Gehrels, W. R., et al. (2016). Temperature-driven global sea-level variability in the Common Era. *Proc Natl Acad Sci USA*, **113** (11) E1434-E1441. doi: 10.1073/pnas.1517056113. Data retrieved 2022-03-16.

35. Clark, P., Shakun, J., Marcott, S., Mix, A., Eby, M., Kulp, S., et al. (2016). Consequences of Twenty-First-Century Policy for Multi-Millennial Climate and Sea-Level Change. *Nature Climate Change*, **6** 10.1038/nclimate2923. Data retrieved from https://www.climatelevels.org/ and https://www.temperaturerecord.org/#sources, 2022-11-23.

36. Moberg, A., Sonechkin, D., Holmgren, K., Datsenko, N. M., Karlén, W., & Lauritzen, S.E. (2006). Correction: Corrigendum: Highly variable Northern Hemisphere temperatures reconstructed from low- and high-resolution proxy data. *Nature*, **439**, 1014. 10.1038/nature04575. Data retrieved from https://www.climatelevels.org/ and https://www.temperaturerecord.org, 2022-11-23.

37. GISTEMP Team. (2022). GISS Surface Temperature Analysis (GISTEMP), version 4. *NASA Goddard Institute for Space Studies*. Dataset accessed 2022-11-23 at nasa.gov/gistemp/, https://search.r-project.org.

38. Lenssen, N., Schmidt, G., Hansen, J., Menne, M., Persin, A., Ruedy, R., & Zyss, D. (2019). Improvements in the GISTEMP uncertainty model. *J. Geophys. Res. Atmos.*, **124**, no. 12, 6307-6326. doi:10.1029/2018JD029522.

39. de Boer, B., van de Wal, R.S.W., Bintanja, R., Lourens, L., & Tuenter, E. (2010). Cenozoic global ice-volume and temperature simulations with 1-D ice-sheet models forced by benthic d18O records. *Ann. Glaciol.* **51**(55), 23–33. doi:10.3189/172756410791392736.

40. Miller, K.G., Browning, J.V., Schmelz, W. J., Kopp, R.E., Mountain, G.S., & Wright, J.D. (2020). Cenozoic sea-level and cryospheric evolution from deep-sea geochemical and continental margin records. *Sci. Adv.*, **6**, eaaz1346. doi: 10.1126/sciadv.aaz1346.

41. Gebbie, G., & Huybers, P. (2019). The Little Ice Age and 20th-century deep Pacific cooling. *Science*, **363**(6422), 70-74. doi: 10.1126/science.aar8413 . PMID: 30606843.

42. Zanna, L., Khatiwala, S., Gregory, J. M., Ison, J., & Heimbach, P. (2019). Global reconstruction of historical ocean heat storage and transport. *Proc Natl Acad Sci USA*, **116** (4) 1126-1131. doi: 10.1073/pnas.1808838115.

43. Kuhlbrodt, T., &Gregory, J. M. (2012). Ocean heat uptake and its consequences for the magnitude of sea level rise and climate change. *Geophys. Res. Lett.*, ***39***, L18608. doi:10.1029/2012GL052952.

44. Levitus, S., Antonov, J. I., Boyer, T. P., Baranova, O. K., Garcia, H.E., Locarnini, R. A., et al. (2012). World ocean heat content and thermosteric sea level change (0–2000 m), 1955–2010. *Geophys. Res. Lett.*, **39**, L10603, doi: 10.1029/2012GL051106.

45. NASA's Goddard Space Flight Center. (2022). Sea Level. https://climate.nasa.gov, last retrieved 2022-11-23.

46. Fox-Kemper, B., Hewitt, H. T., Xiao, C., Aðalgeirsdóttir, G., Drijfhout, S. S., Edwards, T.L., et al. (2021). Ocean, Cryosphere and Sea Level Change. In Climate Change 2021: The Physical Science Basis. Contribution of Working Group I to the Sixth Assessment Report of the Intergovernmental Panel on Climate Change [Masson-Delmotte, V., Zhai, P., Pirani, A., Connors, S. L., Péan, C., et al. (eds.)]. *Cambridge University Press, Cambridge, United Kingdom and New York, NY, USA*, pp. 1211–1362. doi: 10.1017/9781009157896.011.

47. Sweet, W. V., Hamlington, B. D., Kopp, R. E., Weaver, C. P., Barnard, P. L., Bekaert, D., et al. (2022). Global and Regional Sea Level Rise Scenarios for the United States: Updated Mean Projections and Extreme Water Level Probabilities Along U.S. Coastlines. NOAA Technical Report NOS 01. *National Oceanic and Atmospheric Administration, National Ocean Service, Silver Spring, MD*, 111 pp. https://oceanservice.noaa.gov.

48. Horton, B. P., Khan, N. S., Cahill, N., Lee, J. S. H, Shaw, T. A., Garner, A. J., et al. (2020). Estimating global mean sea-level rise and its uncertainties by 2100 and 2300 from an expert survey. *npj Clim Atmos Sci*, **3**, 18. doi: 10.1038/s41612-020-0121-5.

49. Jevrejeva, S., Jackson, L. P., Grindsted, A., Lincke, D., & Marzeion, B. (2018). Flood damage costs under the sea level rise with warming of 1.5 ◦C and 2 ◦C. *Environ. Res. Lett.*, **13** (7), 074014. doi: 10.1088/1748-9326/aacc76.

50. Grinsted, A., & Christensen, J. H. (2021). The transient sensitivity of sea level rise. *Ocean Sci.*, **17**, 181–186. doi: 10.5194/os-17-181-2021.

51. Storto, A., Bonaduce, A., Feng, X., & Yang, C. (2019). Steric Sea Level Changes from Ocean Reanalyses at Global and Regional Scales. *Water*, **11**(10):1987. doi: 10.3390/w11101987.

52. Erban, L. E., Gorelick, S. M., & Zebker, H.A. (2014). Groundwater extraction, land subsidence, and sea-level rise in the Mekong Delta, Vietnam. *Environ. Res. Lett.*, **9** 084010. doi: 10.1088/1748-9326/9/8/084010.

53. Aobpaet, A., Cuenca, M. C., Hooper, A., & Trisirisatayawong, I. (2013). InSAR time-series analysis of land subsidence in Bangkok, Thailand. *International Journal of Remote Sensing*, Vol. **34**, No. 8, 20 April 2013, 2969–2982. doi: 10.1080/01431161.2012.756596.

54. Abidin, H. Z., Andreas, H., Gumilar, I., & Brinkman, J. J. (2015). Study on the risk and impacts of land subsidence in Jakarta. *Proc. IAHS*, **372**, 115–120. doi: 10.5194/piahs-372-115-2015.

55. Abidin, H. Z., Hasanuddin, Z., Supriyadi, S., Gumilar, I., Yuwono, B., & Murdohardono, D. (2015). On Integration of Geodetic Observation Results for Assessment of Land

Subsidence Hazard Risk in Urban Areas of Indonesia. In: Rizos C, Willis P (eds) IAG 150 Years. *International Association of Geodesy Symposia*, vol **143**. Springer, Cham. doi: 10.1007/1345_2015_82.

56. Tay, C., Lindsey, E., Chin, S. T., McCaughey, J. W., Bekaert, D., Nguyen, M., et al. (2022). Sea-level rise from land subsidence in major coastal cities. *Nat Sustain*, **5**, 1049–1057. https://doi.org/10.1038/s41893-022-00947-z.
57. Hoornweg, D., & Pope, K. (2014). Socioeconomic Pathways and Regional Distribution of the World's 101 Largest Cities. Global Cities Institute Working Paper No. 04. *Global Cities Institute (GCI)*.
58. Qu, Y., Liu, Y., Jevrejeva, S., & Jackson, L. P. (2020). Future sea level rise along the coast of China and adjacent region under 1.5 °C and 2.0 °C global warming. *Advances in Climate Change Research*, Volume **11**, Issue 3, Pages 227-238, ISSN 1674-9278. 10.1016/j.accre.2020.09.001.
59. Dunn, R. J. H, Alexander, L. V., Donat, M. G., Zhang, X., Bador, M., Herold, N., et al. (2020). Development of an updated global land in-situ-based dataset of temperature and precipitation extremes: HadEX3. *JGR: Atmospheres*, **125**, e2019JD032263. doi: 10.1029/2019JD032263. Data retrieved from https://www.climdex.org/access/, 2022-10-09.
60. Donat, M. G., Alexander, L. V., Yang, H., Durre, I., Vose, R., & Caesar, J. (2013). Global Land-Based Datasets for Monitoring Climatic Extremes. *Bull. Amer. Meteor. Soc.*, **94**, 997–1006. doi: 10.1175/BAMS-D-12-00109.1. Data retrieved from https://www.climdex.org/access/, 2022-10-09.
61. Morice, C. P., Kennedy, J. J., Rayner, N. A., & Jones, P. D. (2012). Quantifying uncertainties in global and regional temperature change using an ensemble of observational estimates: The HadCRUT4 dataset. *J. Geophys. Res.*, **117**, D08101, doi: 10.1029/2011JD017187. Data retrieved from https://ourworldindata.org, 2022-10-10.
62. McKinsey & Company (2009) Pathways to a Low-Carbon Economy, Version 2 of the Global Greenhouse Gas Abatement Cost Curve. . pathways_lowcarbon_economy_version2. Last accessed 12-Dec-2021.
63. Traber, T., Hegner, F. S., & Fell, H. J. (2021). An Economically Viable 100% Renewable Energy System for All Energy Sectors of Germany in 2030. *Energies* **14**, 5230. https://doi.org/10.3390/en14175230.
64. Traber, T., Fell, H. J., & Marquitan, S. (2021). A full supply with 100% renewable energies including storage is already competitive today and would reduce energy costs. The German example. *Energy Watch Group (EWG)*. https://www.energywatchgroup.org, retrieved 2022-09-01.
65. Kost, C., Shammugam, S., Fluri, V., Peper, D., Memar, A. D., & Schlegel, T. (2021). Levelized cost of electricity. Renewable energy technologies. *Fraunhofer Institute for Solar Energy Systems ISE*. https://www.ise.fraunhofer.de, retrieved 2022-09-01.
66. Roy, N., Burtraw, D., & Rennert, K. (2022). Retail Electricity Rates under the Inflation Reduction Act of 2022. *Resources for the future*. https://www.rff.org, retrieved 2022-09-02.
67. Energie-Control Austria, The Hungarian Energy, Public Utility Regulatory Authority VaasaETT. (2022). Household Energy Price Index for Europe. March 1, 2022. *Household Energy Price Index*. https://www.energypriceindex.com/, retrieved 2022-09-01.

68. IEA International Energy Agency. (2019). Global Energy & CO2 Status Report 2019. Emissions. *IEA Publications*. https://www.iea.org.

69. The World Bank. (2022). Population, total. *World Bank Group*. https://data.worldbank.org. Data retrieved 2022-10-25.

70. Ritchie, H., Roser, M., & Rosado, P. (2022). Global direct primary energy consumption. *Our WorldInData.org. Energy*. Data retrieved from https://ourworldindata.org/grapher/global-primary-energy, 2022-12-01.

71. The World Bank. GDP (constant 2015 US$). (2022). *World Bank Group*. https://data.worldbank.org. Data retrieved 2022-10-25.

72. Ritchie, H., Roser, M., & Rosado, P. (2022). Global CO_2 emissions from fossil fuels and land use change, World. *Our WorldInData.org. Energy*. https://ourworldindata.org. Data retrieved 2022-01-28.

73. Ritchie, H., Roser, M., & Rosado, P. (2022). Annual CO_2 emissions from cement. *Our WorldInData.org. Energy*. https://ourworldindata.org. Data retrieved 2022-01-29.

74. IEA International Energy Agency. (2022). Total energy supply (TES) by GDP. *IEA Data Services*. https://www.iea.org. Data retrieved 2022-11-30.

75. IEA International Energy Agency. (2020). Special Report on Carbon Capture Utilisation and Storage, CCUS in clean energy transitions. Energy Technology Perspectives 2020. *IEA Publications*. https://iea.blob.core.windows.net. Retrieved 2022-12-10.

76. Hendriks, C., Graus, W., & van Bergen, F. (2004). Global carbon dioxide storage potential and costs. *Ecofys, TNO-NITG*. Retrieved from https://www.researchgate.net, 2022-12-10.

77. Johnsson, F., Normann, F., & Svensson, E. (2020). Marginal Abatement Cost Curve of Industrial CO2 Capture and Storage – A Swedish Case Study. *Frontiers in Energy Research*, Vol. **8**. doi: 10.3389/fenrg.2020.00175.

78. NAVIGANT. (2018). Onderbouwing investeringen voor emissiereductie industrie 2030. NAVIGANT. *NAVIGANT CONSULTING, INC*. Retrieved from https://www.klimaatakkoord.nl, 2022-12-10.

79. Lange, G. M., Hamilton, K., Ruta, G., Chakraborti, L., Desai, D., Edens, B., et al. (2011). The changing wealth of nations: measuring sustainable development in the new millennium (English). *World Bank Group, Environment and development*. http://documents.worldbank.org/, last accessed 2023-01-04.

80. Alves, B. (2022). Global flood economic losses 2021, by type. *Statista, Energy & Environment, Climate and Weather*. https://www.statista.com/, last accessed 2023-01-04.

81. NOAA National Centers for Environmental Information (NCEI). (2023). U.S. Billion-Dollar Weather and Climate Disasters. doi: 10.25921/stkw-. 7w73. https://www.ncei.noaa.gov/access/billions/time-series, last accessed 2023-03-13.

82. Wen, S., Su, B., Wang, Y., Fischer, T., Li, X., Yin, Y., et al.(2018). Economic sector loss from influential tropical cyclones and relationship to associated rainfall and wind speed in China. *Global and Planetary Change* **169**, 224-233. doi: https://doi.org/10.1016/j.gloplacha.2018.08.004.

83. Wikipedia. (2023). Tropical cyclones by year. https://en.wikipedia.org/wiki/Tropical_cyclones_by_year, last accessed 2023-03-13.

84. European Environment Agency. (2020). Economic losses from climate-related extremes in Europe. https: direct-losses-from-weather-disasters-3/assessment-2, last accessed 2023-03-13.

85. European Environment Agency. (2022). Annual economic damage caused by weather and climate-related extreme events in the EU Member States. https: natural-disasters-events-5, last accessed 2023-03-13.

86. U.S. Global Change Research Program. (2007). Observed Trends in Hurricane Power Dissipation. https: observed-trends-hurricane-power-dissipation, last accessed 2023-03-13.

87. Knutson, T. R., McBride, J. L., Chan, J., Kerry, E., Holland, G., Landsea, C., et al. (2010). Tropical cyclones and climate change. *Nature Geosci* **3**, 157–163. https://www.nature.com/articles/ngeo779. doi: https://doi.org/10.1038/ngeo779

88. IPCC. (2007). Summary for Policymakers. In: Climate Change 2007: The Physical Science Basis. Contribution of Working Group I to the Fourth Assessment Report of the Intergovernmental Panel on Climate Change [Solomon S, Qin D, Manning M, Chen Z, Marquis M, Averyt KB, Tignor M, Miller HL (eds.)]. Cambridge University Press, Cambridge, United Kingdom and New York, NY, USA. https: ar4-wg1-spm-1, figure SPM.5.

89. Knutson, T., Camargo, S. J., Chan, J. C. L, Kerry, E., Ho, C.-H., Kossin, J., et al. (2020). Tropical Cyclones and Climate Change Assessment: Part II: Projected Response to Anthropogenic Warming. *Bull. Amer. Meteor. Soc.* **101**, E303–E322. doi: https://doi.org/10.1175/BAMS-D-18-0194.1. https: bams-d-18-0194.1.